

Formation Damage

Pore-Cor Research Suite Application Note 2

Using Pore-Cor to Model Mercury Porosimetry, Absolute Permeability and Formation Damage

Pore-Cor can be used to obtain enhanced information from the mercury intrusion porosimetry of oil-reservoir sandstone core plugs. Although the geometry of the Pore-Cor network is simplistic, it is nevertheless flexible enough to closely simulate the percolations properties of actual sandstone samples. Also, crucially, it makes an allowance for the shielding of large pores by small throats, which is not allowed for in the implicit straight capillary approximations commonly used.

As an example, we show how the method was applied to a core plug supplied by Oil Plus from a Chevron Texaco oil field. It was found that the permeability reduction due to colloid occlusion / formation damage is 'later' (i.e. commences at higher sizes of included species) and then drops faster than the capillary bundle model. The resulting unit cell, when occluded by colloid, shows clearly the blocking of access to large pores by small occluded throats. These effects can now be viewed in virtual reality. Other properties, such as the effect of polymer pore plugging, and the extent of fast wetting of samples, can also be calculated.

Before using Pore-Cor RS on their own samples, all users should work through the Pore-Cor tutorials in the Pore-Cor RS Help system, in particular the Application Tutorial on Porous Rock. This Help system is supplied with the software, and is also downloadable from <http://www.pore-cor.com/downloads.htm> . Attendance at a two-day training course is also recommended.

Introduction

The Pore-Cor void network comprises unit cells with periodic boundary conditions. Each unit cell is made up from up to 1000 cuboidal pores, connected by cylindrical, oval-cross sectioned or slit-shaped throats. Fluid is intruded at the xy plane at maximum z in the $-z$ direction – i.e. from the top surface downwards in Figure 1. The periodic boundary conditions make this equivalent to intruding an infinitely wide and broad sheet, of small depth. Thus although the unit cell is small, this simulation is considered a workable approximation to the experimental intrusion of a sample of larger dimension intruded from all sides.

The package has been enhanced in two main ways. Firstly, the fit to the mercury intrusion curve is now performed using a Boltzmann-annealed Simplex, which moves in four parametric dimensions and three Boolean dimensions{Johnson, Roy, et al. 2003 3862 /id}. The four parameters are (i) the skew of the throat size distribution, (ii) the

skew of the pore size distribution, (iii) the connectivity of the network, and (iv) the short-scale size auto-correlation function. The Boolean dimensions are whether (i) the network has a realisable geometry, (ii) whether the spacing between the features can be adjusted to give the exact experimental porosity, and (iii) whether a non-fragmented network can be generated. The parametric system is ill-behaved, and therefore sensitivity analyses are carried out with respect to different stochastic realizations, and with respect to the variation of the parameters, in pairs, away from the optimum fit point.

Once the three-dimensional structure has been generated, a range of static and mobile wetting and non-wetting fluids can be inserted into it, and the properties of the resulting structure measured. Non-wetting fluids are assumed to enter by ‘piston-like’ flow, such that only one fluid is present in any feature at any one time, whereas wetting fluids can partially fill a feature. The second enhancement is that the distribution of the static and mobile fluids can be viewed in virtually reality. (Examples of structures, with a downloadable virtual reality viewer, are available at

http://www.pore-cor.com/virtual_reality.htm).

The software has already been used successfully for soil [1] and paper coatings [2,3]. In this poster, we demonstrate the method by applying it to a single sample, although its strength comes from comparisons of trends between samples.

Procedure

The exemplar sample was a poorly consolidated, lateral turbidite sandstone. The channel sands were well sorted and mature. The sample was from a depth of 6431.20 feet. Its gas permeability was 3335 mD and porosity 33.4%. The maximum intrusion of mercury into pore volume (as measured at 2015 psi) was 83.5%, and hence its effective, modelled porosity was 27.89 %.

The applied mercury pressures were converted to pore diameters using the Laplace equation, assuming the standard surface tension for mercury and an advancing contact angle of 140° . The mercury intrusion curve was fitted using a Boltzmann-annealed Simplex. Ten fits were carried out for each sample, each involving a different stochastic realization. The resulting fits to the experimental data are shown in Table 1 and Figure 1.

Stoch Realn	Porosity	Throat Skew	Pore skew	log10 (Pore skew)	Conn	Corn level	Distance
1	27.88	0.308	766	2.88	3.80	0.251	0.86
2	27.86	0.509	510	2.71	4.16	0.241	1.19
3	27.88	0.515	611	2.79	4.37	0.242	0.85
4	27.88	0.529	692	2.84	4.33	0.262	1.15
5	27.88	0.321	1491	3.17	4.01	0.303	1.10
6	27.88	0.090	1219	3.09	3.58	0.245	1.09
7	27.88	0.321	1491	3.17	4.01	0.303	1.04
8	27.88	-0.129	571	2.76	3.32	0.274	1.26
9	27.88	0.509	510	2.71	4.16	0.241	1.20
10	27.88	-0.211	1825	3.26	3.19	0.229	0.92

Mean	27.88	0.276	866	2.94	3.89	0.259	1.07
Std devn	0.007	0.273		0.21	0.41	0.026	

Table 1 Fitting parameters for the 10 stochastic realizations, and goodness of fit to experimental intrusion curves, expressed as ‘Distance’.

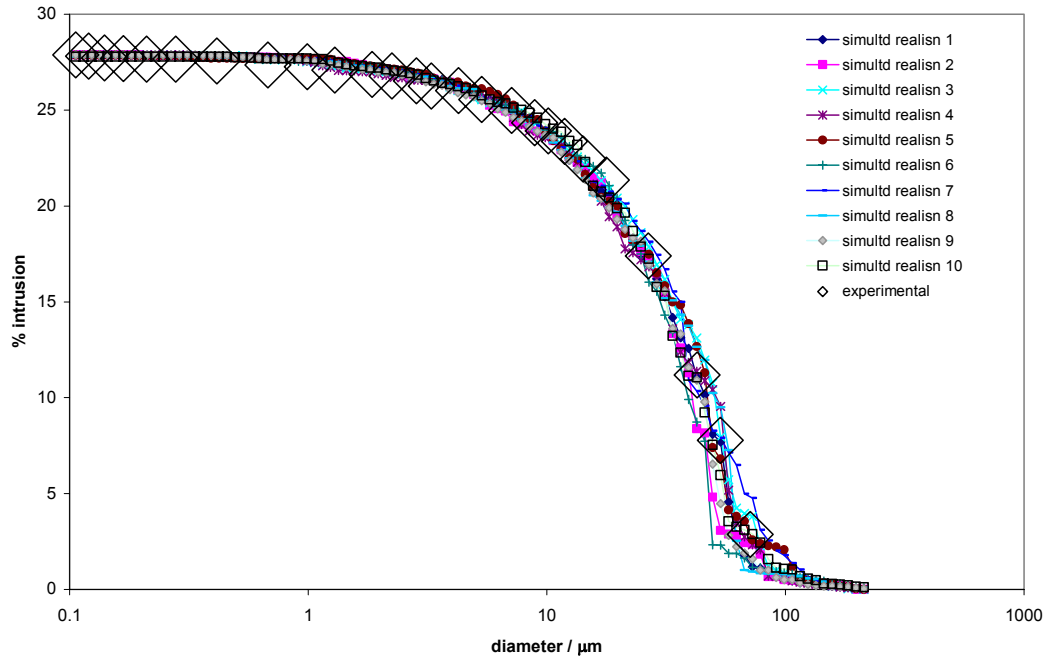


Figure 1 Comparison of experimental and simulated mercury intrusion curves

Note that, importantly, there are no assumptions made by the model of the form of the intrusion curve between experimentally measured points. The simulated curves can take any value between experimental points without penalty as to goodness of fit, and it can be seen that there is consequently a spread between different stochastic realizations at low intrusion pressure / large diameter where there is a sparseness of points.

Figure 2 shows the pore and throat size distributions, expressed as number of features per cubic millimetre of sample, which generate one of the mercury intrusion curves for the sample.

The unit cell of the resulting structure for the first stochastic realization of the sample is shown in Figure 3, with 58.1% of the accessible void volume filled with mercury (shown grey). The scale bar is of length 1 mm. Note that the simulated void structure is not homogeneous – it has slight vertical banding / lamination which is highlighted by the position of the mercury.

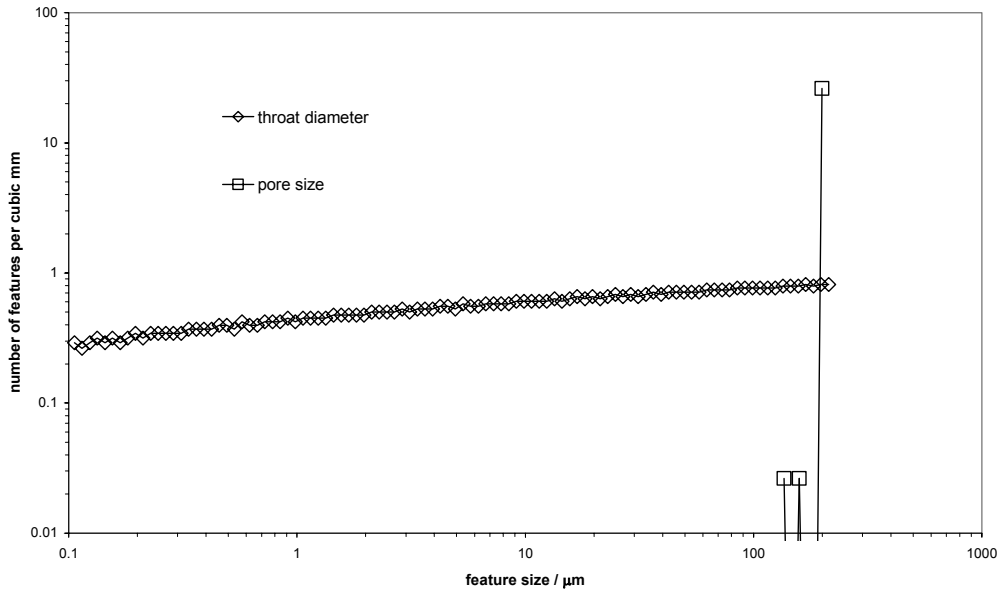


Figure 2 Pore and throat size distributions for one stochastic realization

Results

The effect of occluding the structure is shown in Figure 4, in which the bottom axis shows the maximum allowable particle diameter (MAPD). When compared to the traditional capillary bundle approximation, also shown, the Pore-Cor model suggests a higher diameter can be occluded (a feature of 24 μm, or particle of 8 μm) before permeability reduction is significant, whereupon the permeability reduces more sharply, falling to zero at a particle size between 15 and 18 μm.

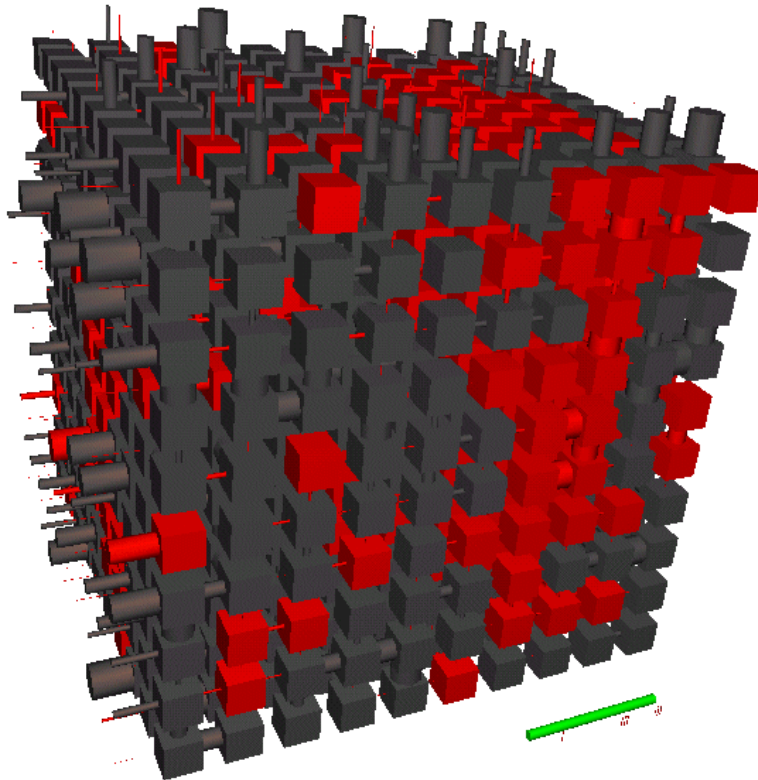


Figure 3 Unit cell of the simulated void structure, 58.1% full of mercury (shown grey)

Figure 5 shows a stochastic realization of the unit cell at the point at which the colloidal inclusions are just severe enough to cause the permeability to drop to zero. The structure has then been intruded with a non-wetting fluid (mercury or oil) shown darker grey, from the top face, to the maximum extent which can be intruded. It can be seen that the extent of intrusion is low, with access to many large pores being blocked by colloidal inclusion of small throats.

Clearly there are variations between stochastic realizations, which would be reduced by the averaging effects of using a larger unit cell. However, there is a clear trend and meaningful average obtained from the present model.

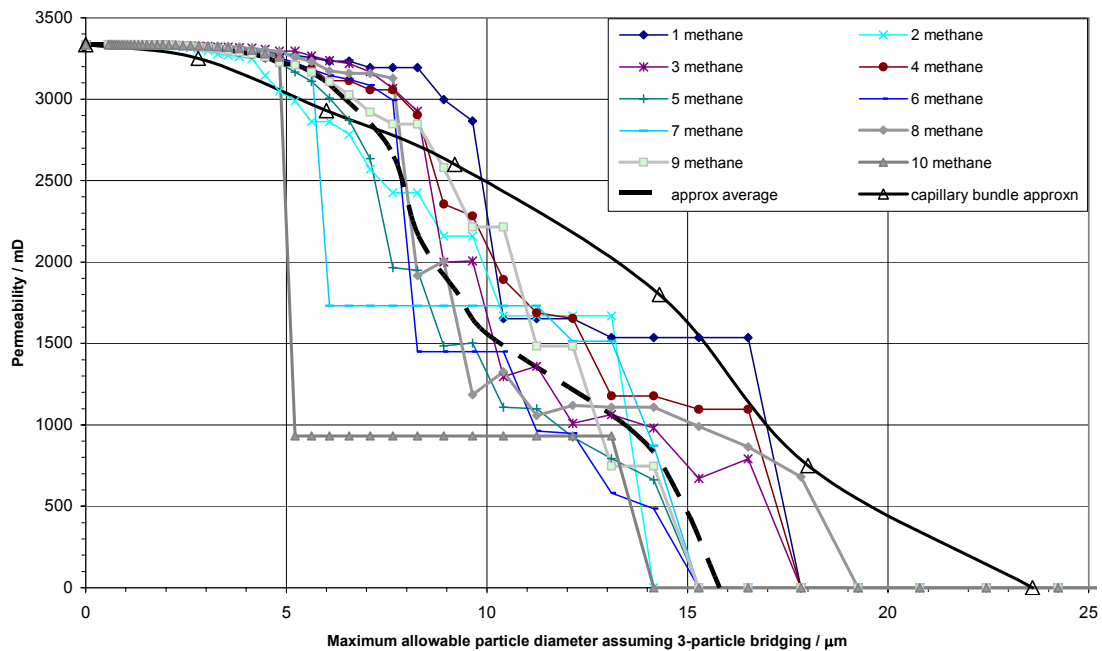


Figure 4 Effect of formation damage shown for 10 stochastic generations and averaged, assuming 3-particle bridging.

Conclusion

- Close fits to the supplied mercury intrusion were achieved for 10 stochastic realizations for each sample.
- The permeability reduction due to colloid occlusion / formation damage is 'later' (i.e. commences at higher sizes of included species) and then drops faster than the capillary bundle model.
- The resulting unit cell, when occluded by colloid, shows clearly the blocking of access to large pores by small occluded throats.
- The distribution of the static and mobile fluids can be viewed in virtually reality.
- Other properties, such as the effect of polymer pore plugging and the extent of fast wetting, can also be calculated.

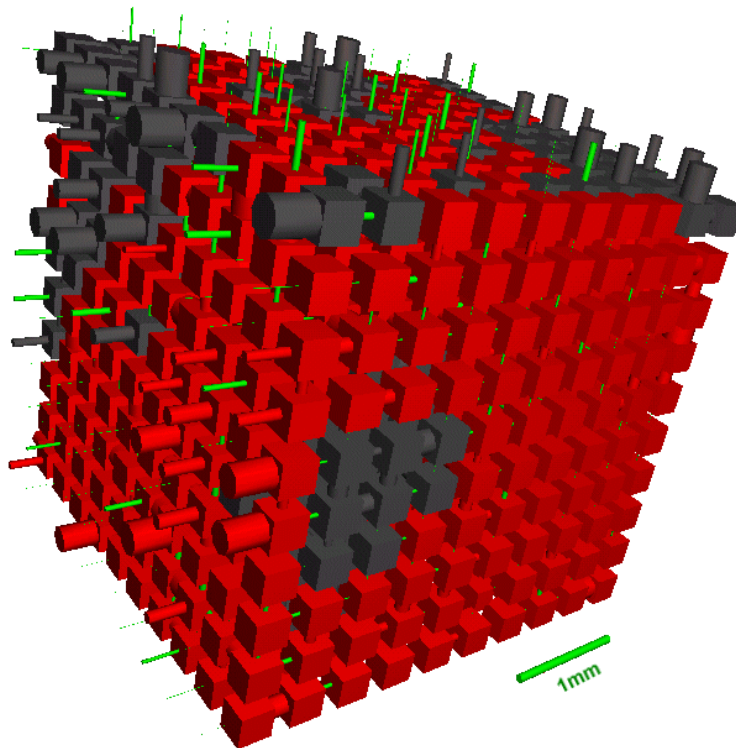


Figure 5 Non-wetting fluid (e.g. oil or mercury) entering the sample, which has its formation damaged just to the extent that its gas permeability has dropped to zero. Increase in pressure on the non-wetting fluid will not increase the intrusion of the non-wetting fluid, unless colloid is displaced.

Acknowledgment

This work was part of a consultancy project commissioned by Oil Plus, Abingdon, UK, for an oilfield operated by Chevron Texaco, and was presented at the Society of Core Analysts International Symposium in Pau, France, September 2003.

References

1. Peat, D M W, Matthews, G P, Worsfold, P J, Jarvis, S C., "Simulation of water retention and hydraulic conductivity in soil using a three-dimensional network", *European J Soil Sci*, (2000) **51**, 65-79.
2. Ridgway, C J, Schoelkopf, J, Matthews, G P, Gane, P A C, James, P W., "The effects of void geometry and contact angle on the absorption of liquids into porous calcium carbonate structures", *J Colloid Interface Sci*, (2001) **239**, 417-431.
3. Schoelkopf, J, Gane, P A C, Ridgway, C J, Matthews, G P., "Practical observation of deviation from Lucas-Washburn scaling in porous media", *Colloids And Surfaces A- Physicochemical And Engineering Aspects*, (2002) **206**, 445-454.